Available online at www.sciencedirect.com
SCIENCE DIRECT®
Microporous and Mesoporous Materials 62 (2003) 61–71
MICROPOROUS AND MESOPOROUS MATERIALS
www.elsevier.com/locate/micromeso

Synthesis and spectroscopic study of mesoporous aluminum methylphosphonate foam templated by dibutyl methylphosphonate

Zongbin Wu [a], Zhongmin Liu [a,*], Peng Tian [a], Yanli He [a], Lei Xu [a], Xiumei Liu [b], Xinhe Bao [b], Xianchun Liu [b]

[a] *Natural Gas Utilization and Applied Catalysis Laboratory, Dalian Institute of Chemical Physics, Chinese Academy of Sciences, P.O. Box 110, Dalian 116023, PR China*

[b] *State Key Laboratory of Catalysis, Dalian Institute of Chemical Physics, Chinese Academy of Sciences, P.O. Box 110, Dalian 116023, PR China*

Received 9 January 2003; received in revised form 28 April 2003; accepted 29 April 2003

Abstract

New types of templates and novel interactive mechanisms between template and framework are very important for creating porous materials. In this work, by using neutral dibutyl methylphosphonate as a template, an inorganic–organic hybrid mesoporous material, aluminum methylphosphonate, was prepared. The as-synthesized material was studied by ^{31}P magnetic angle spinning nuclear magnetic resonance (MAS NMR), ^{27}Al MAS NMR, ^{13}C CP/MAS, FT-IR spectroscopy, thermogravimetry (TG), differential thermal analysis (DTA), and transmission electron microscopy. After thermal treatment at 673 K and 10 mmHg for 2 h, hybrid mesoporous foam was obtained. The transformation process was investigated by FT-IR. TG–DTA results indicate that the methyl group bonded to the framework keeps intact up to 792 K under air and 823 K under nitrogen. The characterization results from nitrogen gas adsorption–desorption measurements show that the BET surface area and the Barrett–Joyner–Halenda desorption cumulative pore volume of the foam are 90 $m^2 g^{-1}$ and 0.32 $cm^3 g^{-1}$ respectively.

Keywords: Aluminum methylphosphonate; Dibutyl methylphosphonate; Foam; Mesoporous; Template

1. Introduction

In recent years, great efforts have been made in the research of inorganic–organic hybrid mesoporous materials. Compared with their inorganic counterparts, hybrid porous materials have many special properties in the areas of catalysis, sorption, storage, and so on [1–5]. Up to now, two predominant methods have been developed for synthesizing inorganic–organic hybrid materials. One is the grafting of the organic groups onto the internal surface of the synthesized inorganic materials [6–9], and the other is to synthesize the hybrid porous materials directly with or without templates [3,5,10–22]. For the first method, it is

* Corresponding author. Tel.: +86-411-468-5510; fax: +86-411-469-1570.
E-mail address: zml@ms.dicp.ac.cn (Z. Liu).

1387-1811/03/$ - see front matter © 2003 Elsevier Inc. All rights reserved.
doi:10.1016/S1387-1811(03)00393-7

convenient to choose a desired inorganic support from the family of porous materials, such as zeolites, zeolite-like materials or amorphous porous materials. However, this method has some problems. For example, it is difficult to modify the internal surface quantitatively and to verify the conformation of the organic moieties precisely. Therefore, more recently, the second method has attracted much interest. Following the principles of coordinate chemistry, the method gives many opportunities for designing a desired structure purposefully. In this way, the open-framework of the inorganic–organic hybrid solids could be an ordered three-dimensional network, with the components assembled together by matching functional groups with or without the assistance of templates. The idea is highlighted by the work of Yaghi's group [3,12]. In the case of using templates, due to the fact that the hybrid framework does not permit high-temperature calcination which is a general method for eliminating the template in zeolites, it is necessary to look for new types of templates which can interact properly with the framework and can be removed easily by soft methods (extraction or evaporation at relatively lower temperatures in vacuum) [9,18]. Due to the important role of templates in the field of porous materials synthesis, new types of templates and novel interactive mechanisms between the template and the framework should be explored seriously. Our interests in the above topics lead us to study the role of neutral phosphonate in the synthesis process of porous aluminum methylphosphonate.

Most of the reported aluminum methylphosphonates have lamellar structures [23–35]. The work of Maeda et al. has shed some light on the synthesis of microporous aluminum methylphosphonates [23,24]. Among the three crystalline phases (AlMepO-α, β, and ξ) reported by Maeda et al., the AlMepO-α and AlMepO-β have a three-dimensional inorganic framework to which the methyl groups are covalently bonded. After a steam treatment of the AlMepO-β at 773 K for 3 h, pure AlMepO-α was obtained with an enhanced adsorption capability. With the methyl groups pointing inwards into the channels, AlMepO-α and AlMepO-β show clearly a hydrophobic nature. Subsequently, a crystalline and fully deuterated phase of AlMepO-β was prepared successfully [25]. By combining the experimental results of nuclear magnetic resonance (NMR) and neutron powder diffraction, the authors found that each of the six crystallographically distinct CD_3 and PO_3 groups adopts a staggered conformation. Besides the microporous aluminum methylphosphonate crystal, the $Al_2(O_3PC_6H_5)\cdot 2H_2O$ seems to have a three-dimensional porous structure [26]. However, nitrogen gas adsorption–desorption isotherms show that no microporous structures are present in the material, and a low specific surface area (25 $m^2\,g^{-1}$) was reported.

In this paper, we report on the template-assisted synthesis of mesoporous aluminum methylphosphonate foam. Dibutyl methylphosphonate (DBMP) was used as the template for the first time. Because DBMP can be removed easily by evaporation at 673 K and 10 mmHg without breaking the P–C bond in aluminum methylphosphonate, it is an ideal agent for use as a template in the synthesis of inorganic–organic hybrid porous materials.

2. Experimental section

2.1. Synthesis of materials

The reagents for the syntheses, such as aluminum nitrate ($Al(NO_3)_3\cdot 9H_2O$, acetonitrile (CH_3-CN), benzene (C_6H_6), methyl iodide (CH_3I), tributyl phosphite ($(CH_3CH_2CH_2CH_2O)_3P$) (TBP), and hydrochloric acid (HCl) are analytically pure.

DBMP: DBMP [dibutyl methylphosphonate, $(CH_3CH_2CH_2CH_2O)_2P(O)(CH_3)$] was prepared according to the Arbusonv rearrangement of TBP [36,37]. Generally, the synthesis process was carried out by dropping methyl iodide into TBP slowly and carefully, and DBMP was obtained almost quantitatively by evaporating the butyl iodide from the mixture at 363 K and 1.5 mmHg.

DMM [mixture of DBMP/MPA (MPA, methylphosphonic acid, $(CH_3)P(O)(OH)_2$)]: Half of the synthesized DBMP was hydrolyzed by refluxing with 6 M HCl for 72 h, and the solution was

evaporated at 383 K to remove water, hydrochloric acid and the by-product 1-butyl chloride. The residue was dissolved in water, treated with charcoal, and filtered. Thus, the MPA aqueous solution was obtained. Another half of the synthesized DBMP was then added to the above aqueous solution. The mixture was evaporated at 383 K and 1.5 mmHg to remove the water. A colorless, transparent and viscous liquid was formed. The liquid (designated as DMM) was a mixture of DBMP and MPA.

AMPF (mesoporous aluminum methylphosphonate foam): Ten gram of aluminum nitrate and 8 ml of DMM were dissolved in 60 ml acetonitrile with stirring. After 30 min, the solution was added dropwise to 60 ml of benzene. A white precipitate was formed when 300 ml of deionized water was added to the above mixture. The precipitate was centrifugalized, washed with deionized water, and dried at 343 K (1.5 mmHg) to produce the as-synthesized aluminum methylphosphonate (designated as AMP). After the AMP was treated at 673 K and 10 mmHg for 2 h to remove the template, the mesoporous aluminum methylphosphonate foam (labeled as AMPF) was formed. The elemental analyses of AMPF gave the following composition (wt.%): C 11.24, H 3.28, Al 10.39, and P 28.80. During the above process, the evaporation products were collected by condensation at 273 K and extracted with 60 ml of water/carbon tetrachloride (CCl_4) (V_{water}:$V_{carbon\ tetrachloride} = 1{:}1$) for three times. The organic phase so obtained was analyzed by GC–MS.

2.2. Characterization of the materials

The C and H contents of the samples were analyzed by an ELEMENTAL ANALYZER-MOD 1106.

DBMP in DMM was analyzed using a HP6890 GC–MS. The gas chromatograph was fitted with a HP5 capillary column (30 m × 0.25 mm). Helium (0.7 ml/min) was used as the carrier gas. The oven was heated at 333 K for 2 min, then the temperature was raised from 333 to 553 K at 10 K/min, and held at 553 K for 20 min. The assignment of the ion current chromatogram was referenced to the Nist98_1 library.

Scanning electron microscope (SEM) image was obtained with a ASID 10 SEM. Transmission electron microscope (TEM) micrographs were obtained by using a TEM JEM-1200EX instrument at 100 kV. The samples were ultrasonically dispersed in deionized water at room temperature for 10 min. A drop of particles dispersed in water was evaporated on a carbon-coated copper grid. Mesoporous size distribution was determined by counting about 50 pores.

^{13}C CP/MAS (MAS, magnetic angle spinning), ^{1}H, ^{31}P and ^{27}Al MAS NMR were recorded at room temperature on a Bruker DRX-400 spectrometer with BBO MAS probe, and a resonance frequency of 400.1 MHz was used for ^{1}H, 128.4 MHz for ^{13}C, 161.9 MHz for ^{31}P, and 104.3 MHz for ^{27}Al. The magnetic field was 9.4 T. The spin rates of the sample were 8, 4, 6 and 8 kHz, and the number of scans was 200, 2084, 100 and 100 for ^{1}H, ^{13}C, ^{31}P and ^{27}Al, respectively. The chemical shifts were referenced to the saturated aqueous solution of sodium 4,4-dimethyl-4-silapentane sulfonate (DSS) for ^{1}H and ^{13}C, 85% H_3PO_4 for ^{31}P, and 1 M aqueous aluminum nitrate for ^{27}Al.

FT-IR spectra were measured on a Bruker EQUINOX 55 FT-IR spectrometer with a resolution of 4 cm^{-1}. For DBMP, AMP and AMPF, potassium bromide (KBr) was used as the support and pure KBr pellet was used as the background. In order to investigate the process of template removal in AMP, a sample was pelletized with fumed silica (mass ratio m_{sample}:$m_{fumed\ silica} = 1{:}50$). The reference substance was a pure fumed silica pellet. The pellet was put into a special sample cell [38], heated at different temperatures (from 473 to 773 K) for 2 h in vacuum (10 mmHg), and then cooled to ambient temperature naturally by keeping the same vacuum. All spectra were recorded at ambient temperature.

The powder XRD patterns were recorded with a D/MAX-b X-ray diffractometer with CuKα radiation and operated at 40 kV and 100 mA. The range of scan began at a 2θ of 1.5°.

Thermogravimetric (TG) and differential thermal analysis (DTA) measurements of the samples were recorded on a Perkin Elmer Pyriss TGA and a Perkin Elmer DTA7 equipment separately, with a heating rate of 10 K/min from 323 to 1173 K

under air or nitrogen gas at a flow rate of 20 ml/min.

The nitrogen gas adsorption–desorption isotherm of AMPF was carried out on a Micrometritics ASAP-2010 apparatus at 77 K. Prior to the measurements, the sample was outgassed at 523 K for 6 h.

3. Results and discussion

3.1. Components of DMM

The ^{1}H NMR of DMM shows six well resolved signals at $\delta = 0.94$, 1.40, 1.49, 1.66, 4.02, and 12.35 ppm with the intensity ratio of ≈1.4:0.9:1.6:1.1:0.9:0.7 (Fig. 1). These signals correspond to the hydrogen atoms of a, b, (e + f), c, d and g respectively [23,39,40]. The intensity ratio of a:b:c:d is 1.4:0.9:1.1:0.9, which equals to ≈3:2:2.4:2 in accordance with the ratio of hydrogen atoms in the corresponding groups of DBMP. Judging from the data in the ^{1}H NMR, the estimated ratio of MPA to DBMP is 1.3. The molar ratio leads to a C/H molar ratio of 0.37 corresponding well with the C/H molar ratio of 0.36 calculated from the elemental analysis of DMM.

The as-synthesized DMM was a viscous liquid. However, after three months' standing at room temperature, many colorless, transparent and irregular crystals appeared in the bottom of the liquid. The upper layer of the viscous liquid was drawn out carefully, dissolved in ethanol, and then analyzed by GC–MS. Fig. 2 shows the chromatograms of the sample, together with a full-scan mass spectrum for Peak 3. Referenced to the standard mass spectrum in Nist98_1, the peaks of 1.46, 1.56 and 19.94 min are assigned to water, ethanol, and DBMP respectively. No detectable methylphosphonic acid monobutyl ester, which was another hydrolyzed product of DBMP, could be found. The crystals were centrifugalized and the viscous liquid adhering to the crystal surfaces was adsorbed by filter papers. The elemental analyses of the crystals gave the following molar ratio (H:C:P = 5.1:1.2:0.8). The molar ratio corresponds

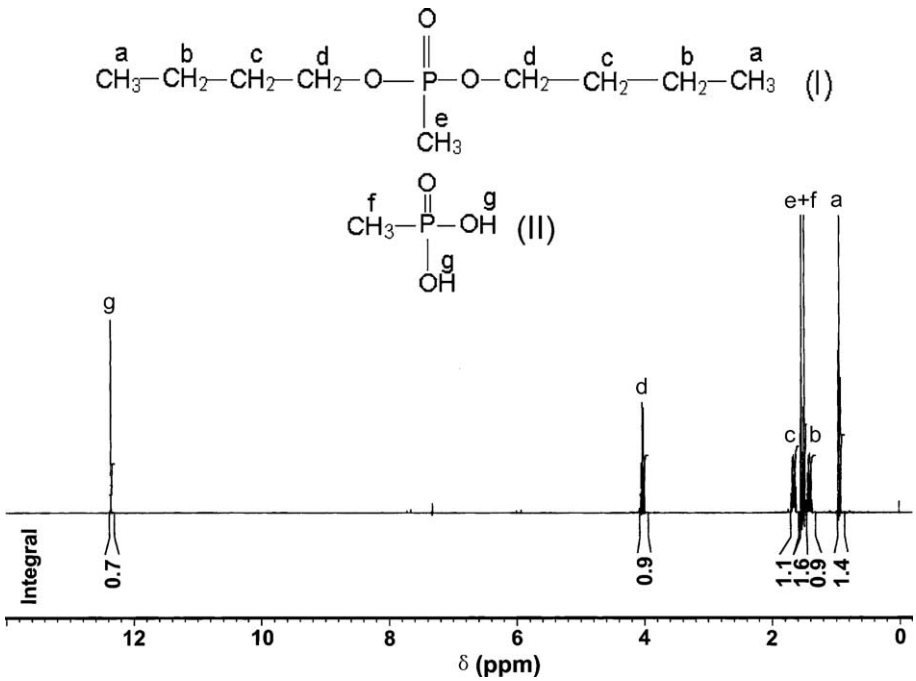

Fig. 1. ^{1}H NMR spectrum of DMM (data measured in $CDCl_3$) with labeled peaks assigned to the corresponding to hydrogen atoms in the structure of DBMP (I) and MPA (II).

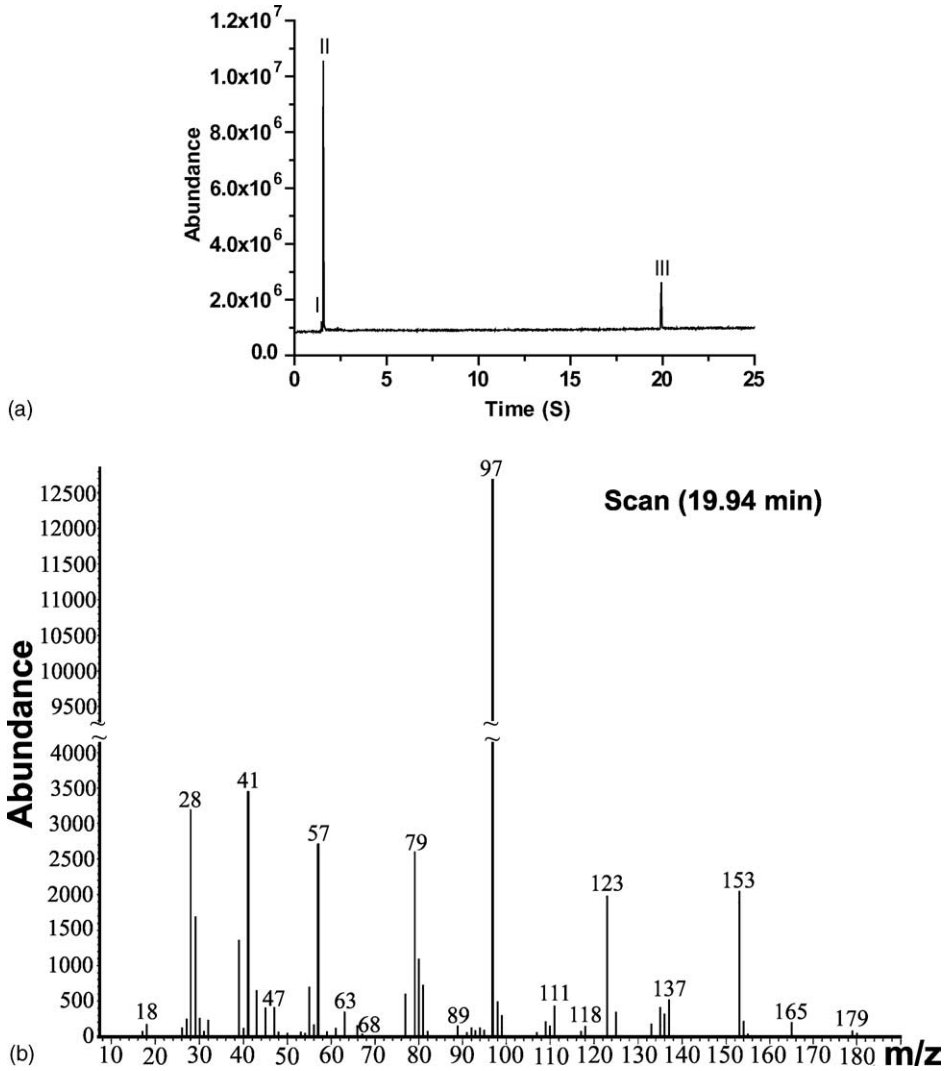

Fig. 2. (a) Reconstructed ion current chromatogram for the upper layer sample dissolved in ethanol (I) water, (II) ethanol, (III) DBMP. (b) Full-scan EI spectrum confirming the identification of DBMP.

well to the ideal molar ratio of MPA (H:C:P = 5:1:1), which ensures that the crystals are MPA. Therefore, the DMM has only two main components, namely DBMP and MPA.

3.2. SEM and TEM images

Fig. 3(a) shows the SEM photograph of AMPF. It could be observed that the AMPF particles are irregular and exhibit a broad distribution of size. The particle morphologies of AMP were also examined by SEM with showing the similar morphologies to that of AMPF (image is not shown). In TEM images, it can be observed that AMP has a complex netted texture (Fig. 3(b)), whereas there are larger pores and mesopores in AMPF (Fig. 3(c) and (d)). Fig. 3(c) shows three-dimensional interconnected larger pores. The size distribution of the larger pore is broad. Based on this image, some mesopores existing in the walls of the larger pores could be observed. To determine the porosity of the walls more easily, Fig. 3(d) was taken

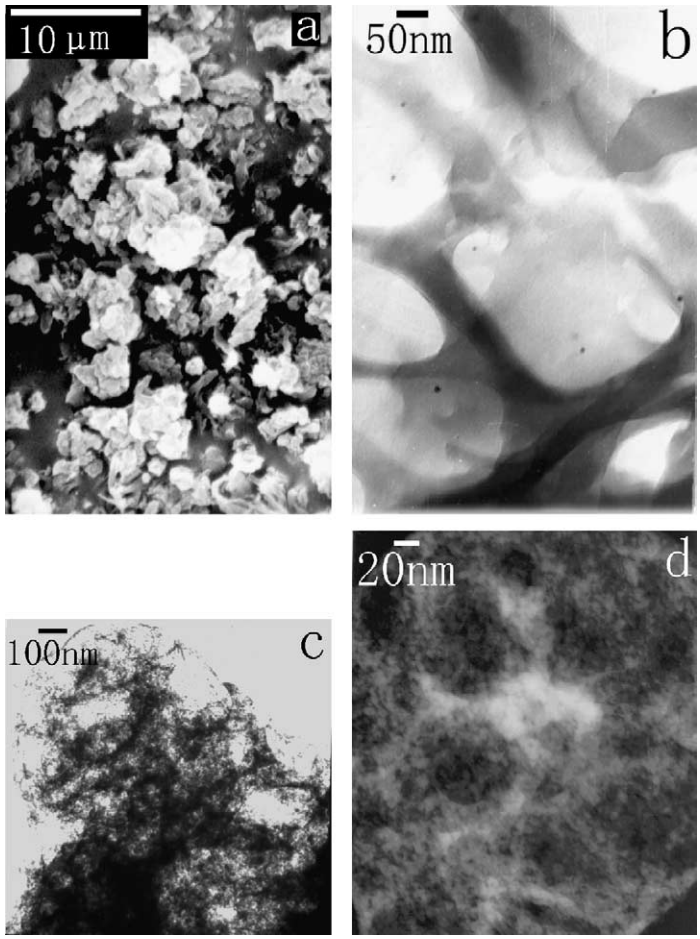

Fig. 3. SEM image of AMPF (a); TEM image of AMP (b); TEM images of AMPF (c,d). (d) is a negative to emphasize the mesopores in the walls.

at a higher magnification. By measuring the diameter of 50 mesopores in Fig. 3(d), the mesopores in the walls have an average diameter of 8 nm.

3.3. Infrared absorption spectra

Table 1 shows the assignments of the characteristic absorption bands of DMM, AMP and AMPF [33,38,41–44]. Some special assignments are discussed as follows.

Compared with free DBMP [45], the frequency of P=O in DMM shifts from 1241 to 1196 cm^{-1}. In DMM, the electron-rich phosphoryl oxygen of DBMP could interact with the hydroxyl group of MPA through the hydrogen bond to give this effect. DBMP combining with MPA directs the reactants to form an interesting netted texture structure shown in the TEM picture. There are four frequency values assigned to the methyl groups in AMPF, namely 2995, 2962, 2933 and 2875 cm^{-1}. This clearly indicates that the methyl groups have different bonding states in the structure.

A thermal treatment of the mixture of the as-synthesized AMP and fumed silica at above 473 K results in a decrease of the intensity of the bands at 2934, 2843, 1465 and 1460 cm^{-1}, corresponding to the methene and methine groups of DBMP (Fig. 4). These bands vanished completely after a treatment at 673 K. The band at 1304 cm^{-1}, as-

Table 1
Spectral data (cm^{-1}) and bond assignment of DMM, AMP, and AMPF[a]

DMM		AMP		AMPF	
IR	Assignment	IR	Assignment	IR	Assignment
2962m	$\nu_{as}CH_3$	2998w	$\nu_{as}CH_3$	2995m	$\nu_{as}CH_3$
2939w	$\nu_{as}CH_2$	2959s	$\nu_{as}CH_3$	2962m	$\nu_{as}CH_3$
2875m	$\nu_{s}CH_3$	2934m	$\nu_{as}CH_2$	2933m	νCH_3
2312w	δP–O–H	2875m	$\nu_{s}CH_3$	2875w	$\nu_{s}CH_3$
1466m	δCH_2	2843w	$\nu_{as}CH_2$	1418m	$\delta_{as}P–CH_3$
1419w	$\delta_{as}P–CH_3$	1465w sh	δCH_2	1314s	$\delta_{s}P–CH_3$
1393w	δP–O–H	1460w	δCH	1101s br	νPO_3
1382w	$\nu_{s}CH_3$	1418w	$\delta_{as}P–CH_3$		Al–O
1315s	$\delta_{s}P–CH_3$	1384m	$\nu_{s}CH_3$	965w br	νAl–O
1196s br	νP=O	1304s	$\delta_{s}P–CH_3$	888m	νAl–O–P
1114w	$\nu_{as}PO_3$	1176vs	$\delta_{as}PO_2$	798s	νAl–O–P
1126w	$\nu_{as}PO_3$	1110s sh	$\delta_{s}PO_2$	656m br	νAl–O–P
1061w	$\nu_{s}PO_3$	1070m	Al–O	505m	δPO_3
1023w	νP–O–C		$\delta_{s}PO_2$	455w	
1002s br	νP–O	1005m	νPO		
912w	$\nu_{s}PO_2$	984s	νP–O–C		
874w		915s	νAl–O–P		
804w		797s	νAl–O–P		
758m	νP–O	572m	$\delta_{as}PO_3$		
482m	$\delta_{as}PO_3$	520w			
427w		484m	$\delta_{s}PO_3$		
		416w			

[a] Relative intensity: v, very; s, strong; m, medium; w, weak; sh, shoulder; br, broad.

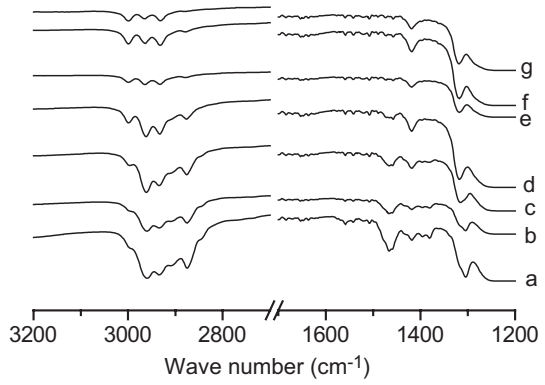

Fig. 4. FT-IR spectra of AMP heat-treated at various temperature for 2 h at 10 mmHg: (a) 473, (b) 523, (c) 573, (d) 623, (e) 673, (f) 723, (g) 773 (K).

signed to P–CH_3, shifts to 1318 cm^{-1} at 523 K, which also indicates the transformation of the framework. Furthermore, the GC–MS result of the extracted sample collected during the preparation of the AMPF shows that DBMP is the main component and no butyl alcohol ($C_4H_{10}O$), which is a decomposition product of DBMP, was observed. Therefore, the conclusion can be drawn that DBMP acts as a template and can be removed in the molecular form by vacuum evaporation.

3.4. NMR spectra

^{13}C CP/MAS NMR spectra of the as-synthesized AMP and AMPF are shown in Fig. 5(a). The AMP exhibits five peaks at 63, 33, 19, 14 and 11 ppm. The former three peaks can be assigned to O$\underline{C}H_2$, $\underline{C}H_2$, and $\underline{C}H_2CH_3$ (labeled by underline) in DBMP conveniently. The last two overlapping peaks should contain the other peaks in DBMP ($\underline{C}H_3$ and P$\underline{C}H_3$) and MAP (P$\underline{C}H_3$). In the spectrum of AMPF, the peaks assigned to DBMP disappeared and only a peak at 14 ppm is assigned to the methyl group. That is to say, DBMP has been eliminated. This conclusion is also supported by the results of the elemental analysis of AMPF with a C/H molar ratio of 0.29 corresponding to the C/H molar ratio of 0.33 in $(CH_3)PO_3$.

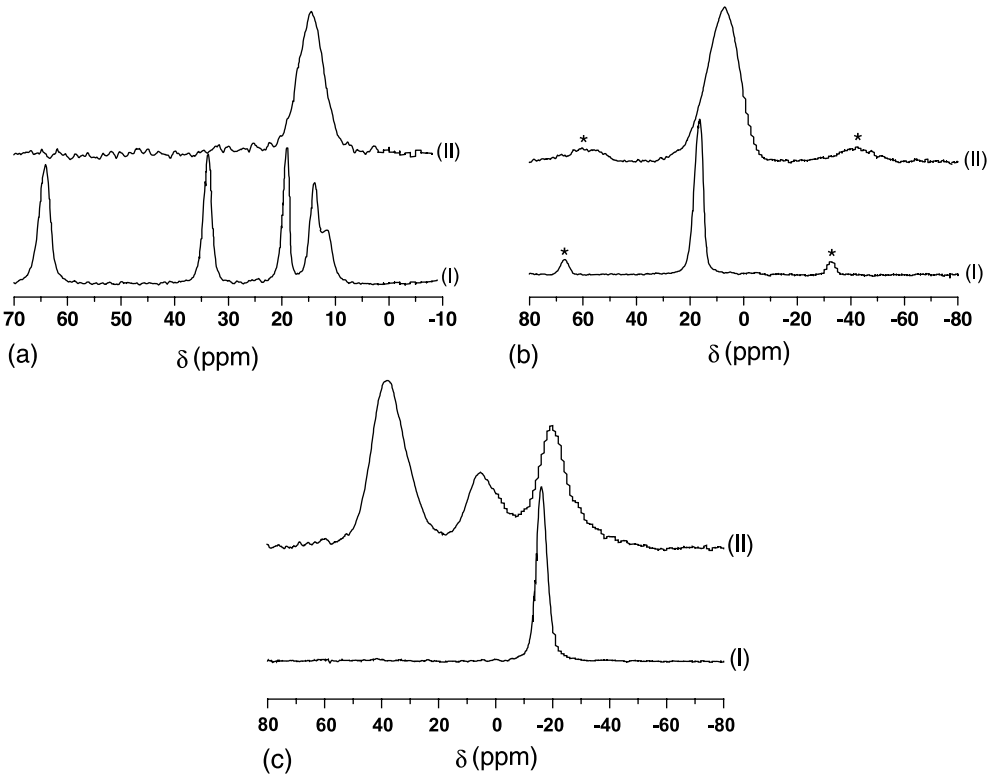

Fig. 5. ^{13}C CP/MAS NMR (a), ^{31}P MAS NMR (b) and ^{27}Al MAS NMR (c) spectra of AMP and AMPF. (I) AMP, (II) AMPF (∗: sidebands).

The ^{31}P MAS NMR spectra of the as-synthesized AMP and AMPF are shown in Fig. 5(b). Free MPA gives a sharp peak at 31 ppm [39], and free DBMP exhibits a peak at ≈34 ppm (this value was obtained from DBMP synthesized in our laboratory), while the as-synthesized DMM gives a predominant peak at 27 ppm and a very weak peak at 30 ppm (figures not shown). This result implies that a strong interaction, namely a hydrogen bond, exists between MPA and DBMP. Such interaction is very important for DBMP in playing the role of template. The as-synthesized AMP gives a sharp and symmetrical peak at 16 ppm. Therefore, in AMP, the coordination environment of phosphorous is symmetrical. After removing DBMP, one broad peak at 7 ppm was observed. The peak shows a broad distribution of P–O–Al angle in AMPF [33].

The observation of the peak of AMP at −16 ppm in the ^{27}Al MAS NMR spectrum (Fig. 5(c)), which is assigned to a six-coordinate aluminum, is in close agreement with the reported value [23,33]. After removing DBMP, the ^{27}Al MAS NMR spectrum changed significantly, with the appearance of three distinct broad peaks at −20, 5, and 38 ppm, which are assigned to six-coordinate, five-coordinate, and four-coordinate aluminum, respectively [23,33,44]. The broadening of the peaks was caused by the disordered structure and the large anisotropic second-order quadrupolar effect.

Summarizing the changes of the spectra due to the thermal treatment, as discussed above, the conclusion is that after the removal of DBMP, the structure of the AMPF is very different from that of the AMP. This is also supported by the XRD patterns (not shown). There are two peaks in the XRD pattern for AMP, the one at 7.8° (2θ) is sharp and intense, and gives an interlayer distance of 11.3 Å, while the other one at 19.7° (2θ) is broad and very weak. However, no peaks are observed in

the XRD patterns of AMPF, which indicates that the structure of AMPF is disordered. Restructuring occurs along with the elimination of the template. The detailed mechanism of the transformation of the structure is unknown yet. Since the mechanism might lead to a novel process characteristic of the template-assisted method, further work should be done to elucidate it.

3.5. Thermal stability

TG–DTA curves of AMP under air and nitrogen are shown in Fig. 6. The initial weight loss (2%) below 472 K, accompanied by an endothermic DTA peak at ≈401 K, is due to the desorbed water. The weight loss (50.9%) caused by the oxidation of DBMP occurs with an exothermic DTA peak at ≈509 K under air, and the corresponding stage under nitrogen is an endothermic DTA peak at ≈607 K produced by the elimination of DBMP. Under air, the weight loss (4.8%) in TG corresponding to two exothermic DTA peaks at ≈792 and 814 K is due to the oxidation of the methyl groups bonded to the framework. However, there are only one endothermic DTA peak at ≈823 K under nitrogen. This difference implies that the methyl groups in aluminum methylphosphonate have different states, which is consistent with the result of FT-IR. The exothermic DTA peak at ≈884 K under air and the endothermic DTA peak at ≈903 K under nitrogen are due to the process of eliminating the remaining hydrogen deficient organic compounds. In the process, very little weight loss was observed, which means that most of the organic components have been removed in the prior stage. From the weight loss of TG, the molar ratio of the methyl groups bonded to the framework to the DBMP is $(m_{\text{methyl}}/\text{Mw}_{\text{methyl}})/(m_{\text{DBMP}}/\text{Mw}_{\text{DBMP}}) = (4.8/15.0)/(50.9/208.4) = 1.3$ (m: mass; Mw: formula weight), which is in agreement with the result of ^{1}H NMR. Based on the above ratio, the deduced value of the C/H molar ratio is 0.41 which corresponds well to the C/H molar ratio of 0.42 calculated from the elemental analysis of AMP. The matching indicates that DBMP keeps its structure intact during the synthesis of AMP and the process of AMPF formation. In other words, DBMP was removed in the molecular form. This is supported by the GC–MS results of the extracted sample collected during the preparation of AMPF.

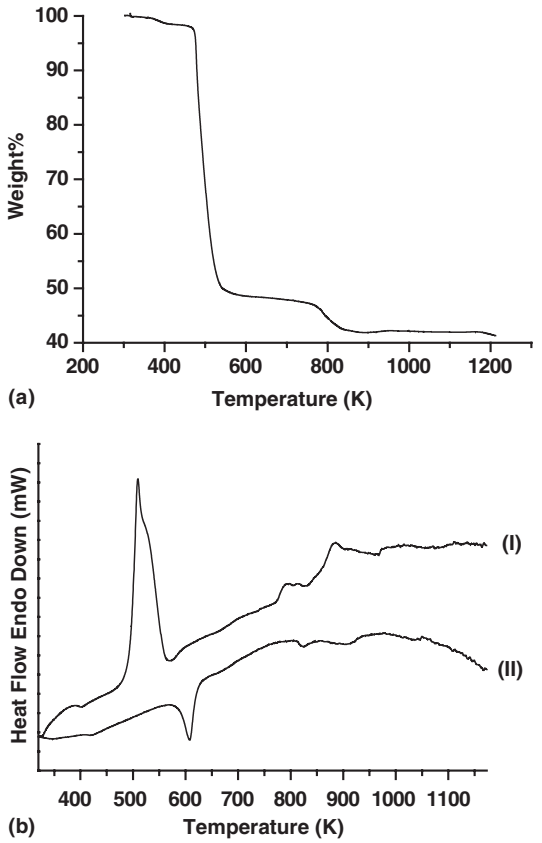

Fig. 6. (a) TG curves of as-synthesized AMP under air. (b) DTA curves of as-synthesized AMP under air (I) and nitrogen (II).

3.6. Nitrogen adsorption–desorption measurement

Information of porosity can be deduced by examining the nitrogen adsorption–desorption isotherm, which is shown in Fig. 7. It is a type IV isotherm and with a broad hysteresis at higher relative pressures, which is typical of mesoporous materials with large pores [46]. A Barrett–Joyner–Halenda (BJH) pore-volume distribution plot from the desorption branch gives a peak at 7.4 nm, close to the observed value by TEM. This shows that the theoretical model is correct. The BET surface area and the BJH desorption cumulative

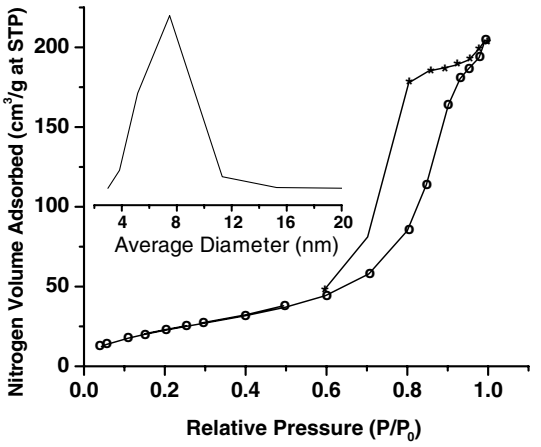

Fig. 7. Nitrogen adsorption–desorption isotherms and pore size distributions (insert) for AMPF (○: adsorption, ∗: desorption).

pore volume of the foam are 90 $m^2 g^{-1}$ and 0.32 $cm^3 g^{-1}$, respectively.

In our subsequent studies, by replacing the aluminum atoms with titanium or zirconium atoms and following the same synthesis process described here, we have successfully synthesized titanium methylphosphonate (designated as TMPF) and zirconium methylphosphonate (designated as ZMPF) open porous materials with BET surface areas of 290 and 279 $m^2 g^{-1}$ respectively. These studies are in progress.

4. Conclusions

Mesoporous aluminum methylphosphonate foam is prepared by using DBMP as the template for the first time. The presence of vibration bands at 2934, 2843, 1465, and 1460 cm^{-1} assigned to methene and methine groups of DBMP makes it convenient to use FT-IR for the study of the process of removing DBMP. After thermal treatment, the above bands vanished completely and porous foam was formed. The BET surface area and the BJH desorption cumulative pore volume of the foam are 90 $m^2 g^{-1}$ and 0.32 $cm^3 g^{-1}$, respectively. Studies with NMR, TG–DTA and TEM also show the great difference in texture between AMP and AMPF. The detailed transformation mechanism is still unknown, but the results described in this paper suggested a promising method for the synthesis of inorganic–organic hybrid porous materials by a novel neutral template, the phosphonate, which can be removed easily without destroying the organic groups bonded to the framework.

Acknowledgements

The authors would like to acknowledge the support of the Knowledge Innovation Program of the Chinese Academy of Sciences (Grant: DICP K2000B3).

References

[1] T. Maschmeyer, F. Rey, G. Sankar, J.M. Thomas, Nature 378 (1995) 159.
[2] K. Maeda, Y. Kiyozumi, F. Mizukami, J. Phys. Chem. B 101 (1997) 4402.
[3] M. Eddaoudi, J. Kim, N. Rosi, D. Vodak, J. Wachter, M. O'keefe, O.M. Yaghi, Science 295 (2002) 469.
[4] S. Natarajan, Proc. Indian Acad. Sci. (Chem. Sci.) 112 (2000) 249.
[5] X. Feng, G.E. Fryxell, L.Q. Wang, A.Y. Kim, J. Liu, K.M. Kemner, Science 276 (1997) 923.
[6] R. Burch, N. Curise, D. Gleeson, S.C. Tsang, Chem. Commun. (1996) 951.
[7] S. Inagaki, S. Guan, Y. Fukushima, T. Ohsuna, O. Terasaki, J. Am. Chem. Soc. 121 (1999) 9611.
[8] T. Asefa, M.J. Maclachlan, N. Coombs, G.A. Ozin, Nature 402 (1999) 867.
[9] X.S. Zhao, G.Q. Lu, J. Phys. Chem. B 102 (1998) 1556.
[10] S. Inagaki, Sh.Y. Guan, T. Ohsuna, O. Terasaki, Nature 416 (2002) 304.
[11] S.S.Y. Chui, S.M.F. Lo, J.P.H. Charmant, A.G. Orpen, L.D. Williams, Science 283 (1999) 1148.
[12] B.L. Chen, M. Eddaoudi, S.T. Hyde, M. O'keefe, O.M. Yaghi, Science 291 (2001) 1021.
[13] T. Asefa, M.J. Maclachlan, H. Grondey, N. Coombs, G.A. Ozin, Angew. Chem. Int. Ed. 39 (2000) 1808.
[14] X.L. Xu, M. Nieuwenhuyzen, S.L. James, Angew. Chem. Int. Ed. 41 (2002) 764.
[15] D.A. Loy, K.J. Shea, Chem. Rev. 95 (1995) 1431.
[16] C.Y. Ishii, T. Asefa, N. Coombs, M.J. Maclachlan, G.A. Ozin, Chem. Commun. (1999) 2539.
[17] M.H. Lim, C.F. Blanford, A. Stein, J. Am. Chem. Soc. 119 (1997) 4090.
[18] C.E. Fowler, B. Lebeau, S. Mann, Chem. Commun. (1998) 1825.
[19] S.R. Hall, C.E. Fowler, B. Lebeau, S. Mann, Chem. Commun. (1998) 1825.

[20] C.E. Fowler, S.L. Burkett, S. Mann, Chem. Commun. (1997) 1769.
[21] D.J. Macquarrie, Chem. Commun. (1996) 1961.
[22] S.L. Burkett, S.D. Sims, S. Mann, Chem. Commun. (1996) 1367.
[23] K. Maeda, Y. Kiyozumi, F. Mizukami, Angew. Chem. Int. Ed. 33 (1994) 2335.
[24] K. Maeda, J. Akimoto, Y. Kiyozumi, F. Mizukami, Angew. Chem. Int. Ed. 34 (1995) 1199.
[25] V.J. Carter, J.P. Kujanpää, F.G. Riddell, P.A. Wright, J.F.C. Turner, C.A.R. Catlow, K.S. Knight, Chem. Phys. Lett. 313 (1999) 505.
[26] A. Cabeza, M.A.G. Aranda, S. Bruque, D.M. Poojary, A. Clearfield, J. Sanz, Inorg. Chem. 37 (1998) 4168.
[27] G.B. Hix, D.S. Wragg, I. Bull, R.E. Morris, P.A. Wright, Chem. Commun. (1992) 2421.
[28] Y. Yang, J. Pinkas, M. Noltemeyer, H.W. Roesky, Inorg. Chem. 37 (1998) 6404.
[29] S.P. Brown, S.E. Ashbrook, S. Wimperis, J. Phys. Chem. B 103 (1999) 812.
[30] D. Chakraborty, S. Horchler, R. Krätzner, S.P. Varkey, J. Pinkas, H.W. Roesky, I. Usón, M. Noltemeyer, H.G. Schmidt, Inorg. Chem. 40 (2001) 2620.
[31] K. Maeda, J. Akimoto, Y. Kiyozumi, F. Mizukami, Chem. Commun. (1995) 1033.
[32] K. Maeda, A. Sasaki, K. Watanabe, Y. Kiyozumi, F. Mizukami, Chem. Lett. (1997) 879.
[33] K. Maeda, Y. Kiyozumi, F. Mizukami, J. Phys. Chem. B 101 (1997) 4402.
[34] K. Maeda, Y. Hashiguchi, Y. Kiyozumi, F. Mizukami, Bull. Chem. Soc. Jpn. 70 (1997) 345.
[35] V.J. Carter, P.A. Wright, J.D. Gale, R.E. Morris, E. Sastre, J.P. Pariente, J. Mater. Chem. 7 (1997) 2287.
[36] D. Redmore, Chem. Rev. 71 (1971) 315.
[37] A.H. Ford-Moore, J.H. Williams, J. Chem. Soc. (1947) 1465.
[38] C. Li, Q. Xin, K.L. Wang, X.X. Guo, Appl. Spectrosc. 45 (1991) 874.
[39] T.G. Appleton, J.R. Hall, A.D. Harris, H.A. Kimlin, I.J. Mcmahon, Aust. J. Chem. 37 (1984) 1833.
[40] M. Handke, M. Rokita, W. Mozgawa, Vib. Spectrosc. 19 (1999) 419.
[41] M. Rokita, M. Handke, W. Mozgawa, J. Mol. Struct. 450 (1998) 213.
[42] L. Bertilsson, K.P. Kamloth, H.D. Liess, I. Engquist, B. Liedberg, J. Phys. Chem. B 102 (1998) 1260.
[43] L.X. Cao, S.R. Segal, S.L. Suib, X. Tang, S. Satyapal, J. Catal. 194 (2000) 61.
[44] H.R. Watling, P.M. Sipos, L. Byrne, G.T. Hefter, P.M. May, Appl. Spectrosc. 53 (1999) 415.
[45] L.L. Burger, J. Phys. Chem. B 62 (1958) 590.
[46] P.A. Webb, C. Orr, Analytical Methods in Fine Particle Technology, Micromeritics Instrument Corporation, Norcross, GA, USA, 1997, pp. 53–59.